Concurrent Imaging for TerraSAR-X: Wide-Area Imaging paired with High-Resolution Capabilities

Thomas Kraus, João Pedro Turchetti Ribeiro, Markus Bachmann, Ulrich Steinbrecher, and Christo Grigorov

Abstract—The concurrent imaging technique enables parallel acquisitions with different beams or modes, e.g., a wide area Stripmap mode with a high resolution Spotlight mode. Such a concurrent Stripmap/Spotlight imaging technique is investigated for TerraSAR-X. This technique employs a pulse-to-pulse interleaving scheme to acquire two acquisitions - even of disjunctive areas - at the same time, offering products with different resolution and coverage portfolios. This capability is especially interesting for customers interested in an overview of a larger area but at the same time observing an area of interest with higher resolution, e.g., for infrastructure monitoring or reconnaissance applications. The basic concept, as well as the driving system parameters, are discussed in detail, together with a coverage analysis revealing the high availability rate of the mode combinations on a global scale. A processing approach reusing a substantial part of the existing infrastructure is described and exemplary acquisitions are shown, together with a detailed performance analysis with respect to resolution and ambiguities.

Index Terms—TerraSAR-X, staring spotlight, concurrent imaging, high resolution, synthetic aperture radar (SAR).

I. INTRODUCTION

TRADITIONAL and state-of-the-art synthetic aperture radar (SAR) sensors operate in well-known imaging modes. They range from high-resolution Spotlight over Stripmap to wide-area ScanSAR modes [1]–[3]. The terrain observation by progressive scans (TOPS) mode can be regarded as an evolution of ScanSAR providing higher quality images at the cost of increased commanding and processing complexity [4], [5]. One common feature of all modes is the tradeoff between resolution and scene size.

The Stripmap (SM) mode allows for continuous imaging in flight direction while providing medium resolution images. The azimuth antenna beam of the SAR is typically looking boresight with respect to the flight direction, i.e., it is not steered. Each point target is illuminated by the radar over an observation angle defined by the width of the azimuth antenna pattern while the sensor is passing by. This angular range directly leads to the achievable azimuth resolution of $\delta_{\mathrm{Az,SM}} = \frac{L}{2}$, where L is the physical size of the SAR antenna in the azimuth direction.

The Staring Spotlight mode (ST) is the Spotlight variant with the highest resolution. It is offering high azimuth resolution while compromising the scene size in flight direction

T. Kraus, M. Bachmann, U. Steinbrecher, and C. Grigorov are with the Microwaves and Radar Institute, German Aerospace Center (DLR), 82234 Oberpfaffenhofen, Germany (e-mail: T.Kraus@dlr.de).

J. P. Turchetti Ribeiro is with the Aeronautics Institute of Technology (ITA), São José dos Campos, Brazil.

[3], [6], [7]. By continuously steering the radar antenna to the center of the scene, the observation time for this area is maximized, leading to the high-resolution radar data. The rotation center is the center of the ST scene. The resolution of the Staring Spotlight mode can be calculated as $\delta_{\mathrm{Az,ST}} = \lambda/(2\Delta\Theta_{\mathrm{a}})$, where λ is the wavelength of the transmitted signal and $\Delta\Theta_{\mathrm{a}}$ is the angular range defined by the azimuth antenna steering. The improved azimuth resolution of the ST mode compared to SM is paid by a smaller scene size as mentioned before. The extent of the resulting scene is limited to the radar antenna beamwidth projected to the ground.

The so-called Sliding Spotlight modes can be regarded as a compromise providing a larger (but still finite) scene size in azimuth at the cost of a lower azimuth resolution compared to ST. During early times, those modes have been called hybrid SAR modes [8], [9]. Depending on the depth of the center of rotation w.r.t. the surface a stronger or slighter sliding can be performed, providing flexibility to the mode design. For the example of the TerraSAR-X mission, two Sliding Spotlight modes are available, the so-called High-Resolution Spotlight mode (HS) and a Sliding Spotlight mode (SL) [10].

An azimuth steerable single-channel SAR system can operate in all these modes; however, under the restriction of using only one at a time for each area of interest. For future SAR systems, highly innovative imaging modes have been developed in order to improve the performance and the flexibility to satisfy ever-growing user demands. Those modes require hardware and processing capabilities way beyond state-of-the-art systems, such as multidimensional waveform encoding and digital beamforming, employing many channels for the receiving chain [11]–[13]. Given those capabilities, not only a single-mode image can be acquired, but two or more images in different imaging modes can be generated simultaneously. This multitude of modes at the same time is also called hybrid operation in [11]. An experimental space-born demonstration of digital beamforming capabilities using the single-channel TerraSAR-X system is reported in [14].

The paper at hand refers to a concurrent imaging technique, which can be regarded as a step towards such a hybrid mode. It goes beyond the Sliding Spotlight approach of the early days but does not address highly innovative beamforming and waveform encoding techniques. The idea is to acquire two images simultaneously, by interleaving the acquisitions in a pulse-to-pulse manner. Like in the well-established scheme for the TerraSAR-X dual or quad polarization acquisitions the transmit and receive configurations of the SAR instrument are toggling [15], [16]. This idea is also described in the literature, where a semi-operational implementation for the

COSMO-SkyMed next-generation constellation is envisaged, focusing on the acquisition of two Spotlight acquisitions at the same time [17]–[20]. Here we address this idea from the TerraSAR-X perspective, where we concentrate on the simultaneous acquisition of a Spotlight and a Stripmap product. Such a mode is favorable where an overview of a wider area is necessary, and in parallel, a zoom on a selected target of interest is required. Applications can range from scientific over civil engineering to military use cases. Additionally, the acquisition over disjoint areas is analyzed which can greatly reduce conflicting mode or scene selections which regularly appear over regions of high interest.

The paper is structured as follows. In Section II, the concurrent imaging technique is described. This covers the basic concept as well as a thorough timing and ambiguity analysis. Section III provides a coverage analysis that gives an idea about the applicability of the investigated scheme for acquisitions all over the Earth. In Section IV, the commanding and processing aspects are treated, followed by experimental results in Section V. Exemplary acquisitions are shown and analyzed with respect to their impulse response function and ambiguity characteristics. In Section VI, further optimization strategies for the concurrent imaging technique are discussed. Finally, Section VII concludes the paper.

II. CONCURRENT IMAGING TECHNIQUE

State-of-the-art imaging modes of single-channel SAR systems so far did not offer any flexibility to acquire high resolution data in a continuous manner nor the ability to acquire two disjunctive scenes simultaneously. There is always a compromise in choosing the right imaging mode for a given application. Azimuth and range resolution have to be traded against scene extent and a single area of interest has to be selected. The flexibility to acquire a high resolution image at the same time as a continuous coverage image or to image more than one area of interest at the moment is paid by dramatically increased hardware and processing complexity for digital beamforming systems. Digital beamforming demands multiple receive channels, which drastically increases the amount of data to be downlinked to the ground. Moreover, spatiotemporal waveform encoding requires additional processing in the transmitter and receiver, creating more complexity for the system. This gap in capabilities for single-channel systems is filled by the concurrent imaging technique described in the next section.

A. Basic Concept

The idea behind this data acquisition scheme is to interleave acquisitions in a pulse-to-pulse manner, taking into account additional constraints arising from this concept. As illustrated in Figure 1, Stripmap and Spotlight images can be acquired simultaneously by continuously switching between image mode acquisition schemes from pulse to pulse. The beams depicted in blue are acquiring the Stripmap data. They have wider coverage in elevation, and the azimuth beam is looking in a boresight direction during the whole acquisition, enabling continuous imaging. The red beams offer a narrower elevation
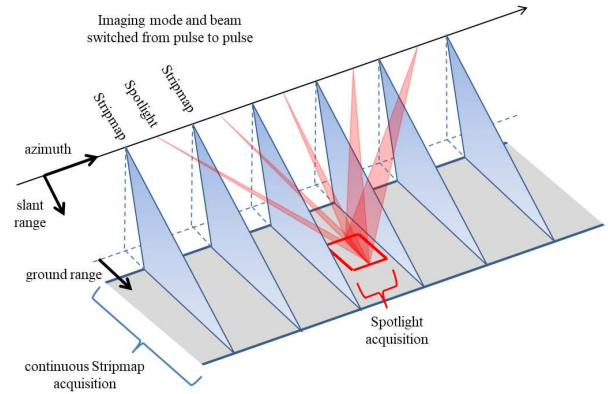

Fig. 1. Schematic representation of the data acquisition and imaging mode, which allows simultaneous acquisition of a Stripmap and a Spotlight scene, by alternating the transmit and receive antenna pattern in elevation and in azimuth, as well as the radiated waveform from pulse to pulse.

scene size, and the azimuth antenna steering is adjusted during the overflight to image the region of interest for a long time, enabling high azimuth resolution. Despite the elevation and azimuth antenna beams, the transmit and the receive bandwidth and the transmitted waveform can be alternated and tailored to the application. State-of-the-art satellite SAR systems such as, e.g., TerraSAR-X, are using a higher RF bandwidth for the Spotlight acquisitions in order to achieve a similarly high range resolution as the high azimuth resolution achieved due to the azimuth antenna steering.

Besides the acquisition of a Spotlight image within a Stripmap one, the acquisition of disjunctive areas is possible. This scheme is presented in Figure 2 for two continuous Stripmap scenes. The elevation beam is switched from pulse to pulse from one swath to the other. However, the acquisition of a Spotlight scene outside the swath of the Stripmap acquisition is possible, too. Experimental results are presented in Section V.

Two major constraints have to be respected when designing a single-channel concurrent imaging SAR acquisition. First, the timing constraints have to be considered. If both images are not in the same range, the selected pulse repetition frequency (PRF) must suit both areas (as shown in Figure 2) for a pair of disjunctive Stripmap acquisitions. However, if both acquisitions are acquired over the same area, as depicted in Figure 1, there is no additional constraint compared to a conventional Stripmap or Spotlight acquisition.

The second constraint on the PRF is that it has to be chosen adequately high, as each of the sub-images is acquired with an effective PRF, $f_{\text{PRF,eff}}$, equal to half the PRF, which is used for the combined Stripmap/Spotlight acquisition $f_{\text{PRF,SM/ST}}$

$$f_{\text{PRF,eff}} = \frac{f_{\text{PRF,SM/ST}}}{2}. \tag{1}$$

The corresponding effective pulse repetition interval (PRI), $T_{\text{PRI,eff}}$, is the sum of the Stripmap PRI, $T_{\text{PRI,SM}}$, and the Staring Spotlight PRI, $T_{\text{PRI,ST}}$

$$T_{\text{PRI,eff}} = \frac{1}{f_{\text{PRF,eff}}} = T_{\text{PRI,SM}} + T_{\text{PRI,ST}}. \tag{2}$$
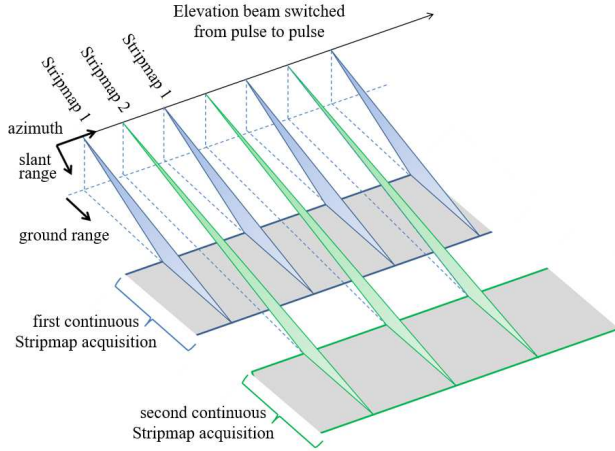
Fig. 2. Schematic representation of the data acquisition and imaging mode by selecting an appropriate PRF. Here the challenge is to use the same echo window for a different number (rank) of traveling pulses, which makes PRF selection more challenging. This configuration allows simultaneous acquisition of two disjunctive Stripmap scenes by alternating the transmit and receive antenna pattern in elevation from pulse to pulse. Also, the second scene could be a Spotlight acquisition.

For the sake of simplicity, the concurrent imaging technique analyzed in this paper and described in [18] assumes the same PRIs for both images

$$T_{\text{PRI,SM}} = T_{\text{PRI,ST}}. \qquad (3)$$

Using different PRIs would offer more flexibility in terms of timing constraints and achievable scene sizes. This approach is discussed in Section VI.

Arising range ambiguities due to high PRF can be tackled by using proper waveform design. For example, orthogonal waveforms can be used, as up and down chirping, in each mode of the combined acquisition, respectively in order to avoid the focusing of ambiguities of point targets [21]. Nevertheless, the energy of the ambiguous pulses is contained in the image and no improvement can be achieved for distributed targets [13], [21].

An additional bounding condition in the TerraSAR-X acquisition is caused by the limitation that the SAR system can only switch antenna beams in transmit and receive independently for nominal imaging modes. For a concurrent Stripmap/Spotlight acquisition, transmitting with one antenna beam and receiving with another during the same PRI is not possible. Thus, the number of traveling pulses has to be even. This ensures the reception of the echoes of each mode with the proper antenna pattern, i.e., right after transmission of the given mode. For a concurrent Stripmap/Stripmap acquisition, it is possible to transmit with a certain elevation beam and receive with another elevation beam within the same PRI. Therefore, an odd number of traveling pulses is also possible which relaxes timing constraints because a wider PRF range is usable.

B. Timing Assessment

Traditional monostatic SAR acquisitions are characterized by transmission in a pulse-wise manner. In other words, the transmission is periodic according to the PRI. Each period consists of an active transmission followed by a reception interval. The antenna is actively transmitting during a time interval of length PRI $times$ duty cycle.

The first timing constraint is that reception is only possible outside the transmission window. This restriction comes from the enormous difference between the high power of the transmit signal and the low power of the echo. Since the same antenna is used to transmit and receive in monostatic systems, the receiver would be saturated and, therefore, would not be able to detect the low power of the echo.

The second constraint is related to the nadir echo, which is the signal received reflected from the Earth around the nadir line. The nadir line is, by definition, the line on Earth's surface of closest approach to the satellite trajectory. Reception of the nadir echoes simultaneously to the target echoes can cause a strong bright line in the focused image due to the small incidence angle and the high backscatter of the nadir area [22], [23]. The reception of nadir echos can be avoided by proper PRF selection.

These two constraints are known as transmission and nadir interference, respectively. They can be summarized by the timing diagram shown in Figure 3 [2]. For the concurrent imaging technique, the combined PRF $f_{\text{PRF,SM/ST}}$ explained in Section II-A must be used in the timing diagram.

The white diamond-shaped areas represent usable PRF regions for scenes seen under a certain incidence angle. The decreasing size of usable areas between transmit and nadir interference lines for higher incidence angles and increasing PRFs is a direct consequence of the acquisition geometry. As shown in the following section, a concurrent acquisition calls for a relatively high PRF which complicates timing as the diamonds become smaller, limiting the achievable scene size.

C. Ambiguity Assessment

Since two images are being acquired in the concurrent imaging mode simultaneously, the PRF must be high enough to ensure a sufficiently high sampling frequency to accommodate both modes with sufficient azimuth bandwidth. This motivates the analysis of range and azimuth ambiguities as these parameters are tightly connected to the PRF. Ambiguities come from different effects:

- Azimuth ambiguities are a result of the sampling of the Doppler spectrum by the PRF. The Doppler spectrum is not strictly band-limited, but shaped by the azimuth antenna pattern. Therefore, there is significant signal energy with Doppler frequencies beyond the sampling frequency (PRF), leading to aliasing.
- Range ambiguities arise because the round-trip delay (between transmission and reception of a pulse) is larger than the PRI. Echoes of subsequent and previous pulses manifest at the same echo window position as the actual intended echo, although their travel time has a multiple PRI difference.
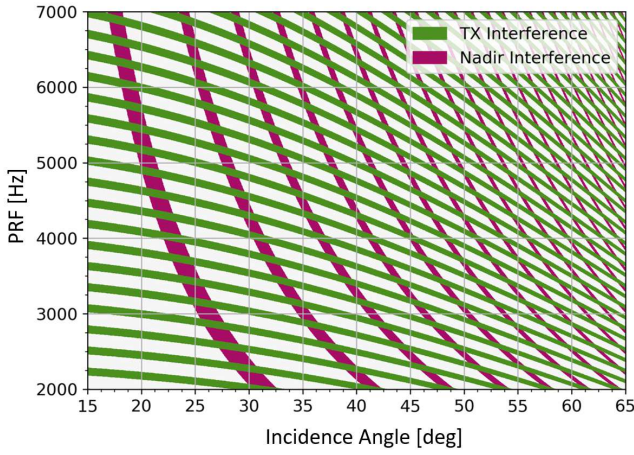
Fig. 3. The timing diagram for an orbit height of 520 km and a transmit duty-cycle of 20%. The green areas indicate transmit interference, and the purple regions indicate nadir interference. Both types of interference need to be avoided by proper PRF selection for an incidence angle of interest. Those usable PRF and incidence angle combinations are shown as diamond-shaped white areas.

The tolerable ambiguity levels depend on the application. For areas with relatively homogeneous backscatter, the ambiguous energy is contributing to the total image noise and visually reduces the contrast of images by turning regions of low backscatter like airport runways into gray areas complicating, e.g., the detection of aircraft [2], [6], [24]. For scenes with high contrast in backscatter the appearance of ghost targets can be problematic. Ships appear as bright targets on a calm sea surface, but their azimuth ambiguities are clearly detectable as well [25].

Since there are two different effects causing ambiguities, it is common practice to assess the ambiguity performance of a SAR system describing azimuth and range ambiguities separately. For antenna systems where the side-lobes are concentrated in the principal planes (e.g., for rectangular planar antennas like TerraSAR-X and TanDEM-X), this approach is regarded as sufficiently precise. As a general rule, increasing the PRF leads to a higher range ambiguity-to-signal ratio (RASR) and a lower azimuth ambiguity-to-signal ratio (AASR). Thereby, an analysis of this trade-off must be carried out to guarantee a minimum of received total ambiguity power and possibly optimum acquisition performance. In order to perform a simulation to assess ambiguities in both range and azimuth, the satellite orbit, attitude, antenna pattern, and the target position must be known.

The RASR is defined as the ratio of the sum of all ambiguous power contributions from M different ambiguous ranges, $P_{\mathrm{amb},m}$, to the power at the target area, P_{target},

$$\mathrm{RASR} = \frac{\sum\limits_{m=1}^{M} P_{\mathrm{amb},m}}{P_{\mathrm{target}}}. \qquad (4)$$

To compute RASR, we need to pay attention to the involved parameters. Some parameters are different for the ambiguity and the target areas (e.g., antenna gain), and others that are the same and will be canceled out (e.g., transmit power, losses, the wavelength). Thus, the RASR can be give by

$$\mathrm{RASR} = \frac{\sum\limits_{m=1}^{M} \dfrac{G_{\mathrm{el,Tx},m} G_{\mathrm{el,Rx},m} \sigma_{0,m}}{\sin\left(\theta_{\mathrm{i},m}\right) R_m^3}}{\dfrac{G_{\mathrm{el,Tx},0} G_{\mathrm{el,Rx},0} \sigma_{0,0}}{\sin\left(\theta_{\mathrm{i},0}\right) R_0^3}}, \qquad (5)$$

where $G_{\mathrm{el,Tx}}$ and $G_{\mathrm{el,Rx}}$ are the transmit and receive antenna pattern gains respectively [2]. The subscripts m and 0 indicate the evaluation of the antenna patterns (and other parameters) for the position of the m-th ambiguity and the target area respectively. The parameter σ_0 is the backscatter coefficient, θ_{i} is the incidence angle, and R is the slant range.

Because there is a cross-interference between the modes, i.e., the Stripmap mode is interfering with the Spotlight and vice versa, one shall use the combined PRF, which is twice the effective PRF, to obtain the ambiguous range positions, and therefore the RASR. This is a worst-case assumption, as Equation 5 is not considering the azimuth antenna pattern and therefore assumes maximum interference between the modes. This is only true when both interleaved modes point to the same area with the maximum of the azimuth antenna pattern, i.e., at the center of the acquisition, when the Spotlight azimuth beam is pointing boresight.

Figure 4 and Figure 5 show the RASR versus the PRF for the Staring Spotlight and the Stripmap, respectively. The general trend of increasing RASR with increasing PRF is clearly visible for both modes. The parameter Δ_{rg} describes the positions of the simulated point targets with respect to the center of the scene in range direction. Especially in the Stripmap mode, where the scene extent in range is substantially larger than in Staring Spotlight, a degraded range ambiguity performance for larger deviations from the scene center is visible in the high PRF region. In Figure 6 the one-way elevation antenna patterns used for the RASR simulations are shown. The strip_011 pattern is tapered to reduce side lobes and widen the beam, because the nominal scene size of Stripmap acquisitions is 30 km, whereas a Spotlight acquisition is maximum 10 km in range. The spot_051 pattern shows a sinc characteristic because it is optimize for maximum gain [26].

For the assessment of the azimuth ambiguity performance, the effective PRF $f_{\mathrm{PRF,eff}}$ has to be used, as both modes experience a sampling of their Doppler spectra with this rate. Additionally, the Stripmap and the Staring Spotlight part have to be treated differently. On the one hand, for Stripmap, there is the possibility to reduce the processed azimuth bandwidth $B_{\mathrm{az,SM}}$ with respect to the PRF to gain AASR performance. This can be described by an azimuth oversampling factor

$$\alpha_{\mathrm{os,a}} = \frac{f_{\mathrm{PRF,eff}}}{B_{\mathrm{az,SM}}}. \qquad (6)$$

This factor clarifies the trade-off between azimuth resolution and azimuth ambiguities in the Stripmap mode. On the other hand, the AASR performance of Staring Spotlight has to be assessed carefully, considering the time-variant azimuth antenna pattern and the weighting of the azimuth spectrum with its processing window. Both aspects have a significant
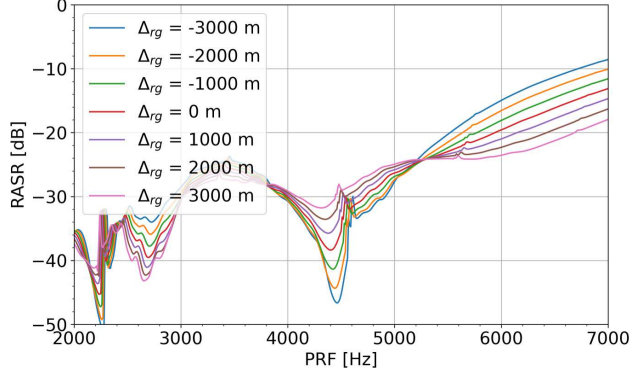
Fig. 4. Simulated RASR for the TerraSAR-X Staring Spotlight mode at different range target positions for the exemplary elevation beam spot_051 with an incidence angle of approximately 40°. The distance of the simulated target with respect to scene center Δ_rg is provided in the legend. In order to respect cross-interference between the modes, the combined PRF needs to be evaluated.
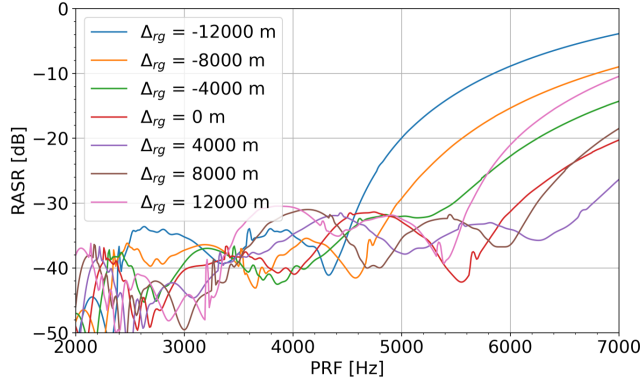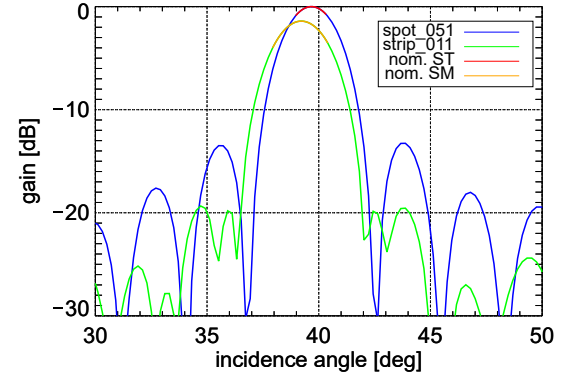

Fig. 6. Elevation antenna pattern (one-way, normalized) used for the RASR simulation. The blue curve represents the elevation beam spot_051 and the green one strip_011, respectively. The regions of the pattern, which are used for nominal Staring Spotlight and Stripmap acquisitions are highlighted in red and orange, respectively.

Fig. 5. Simulated RASR for the TerraSAR-X Stripmap mode at different range target positions for the exemplary elevation beam strip_011 with an incidence angle of approximately 40°. The distance of the simulated target with respect to scene center Δ_rg is provided in the legend. In order to respect cross-interference between the modes, the combined PRF needs to be evaluated.
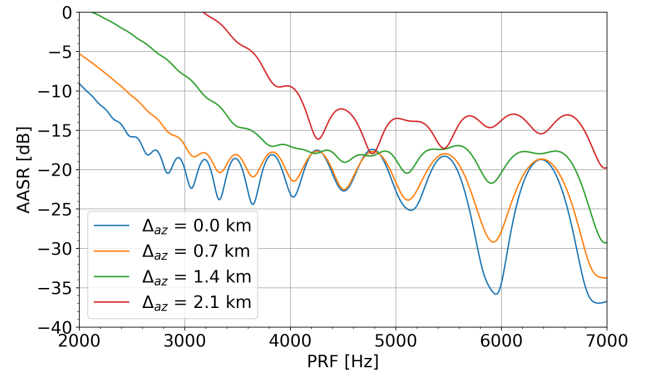

Fig. 7. Simulated AASR for the TerraSAR-X Staring Spotlight mode at different azimuth target positions. Different distances of the simulated target with respect to scene center Δ_az are provided. A generalized Hamming window with $\alpha = 0.6$ and an azimuth antenna steering from -2.2° to 2.2° were used. For the concurrent imaging case, the effective PRF was used.

influence on the achievable performance, as described in detail in [6] and [7]. The AASR of Staring Spotlight can be calculated considering N time steps to account for the time-variant azimuth antenna pattern steering and m as the order of the ambiguity

$$\mathrm{AASR} = \frac{\sum\limits_{n=1}^{N} \sum\limits_{\substack{m=-M \\ m \neq 0}}^{M} P_{\mathrm{amb},n,m} \mathrm{W}_n^2}{\sum\limits_{n=1}^{N} P_{\mathrm{target},n} \mathrm{W}_n^2}, \qquad (7)$$

where for TerraSAR-X a (generalized) Hamming window with $\alpha = 0.6$ is used for spectral weighting

$$\mathrm{W}_n = \alpha - (1-\alpha)\cos\left(\frac{2\pi n}{N}\right), \quad n = 1, ..., N. \qquad (8)$$

Figure 7 and Figure 8 show the AASR performance for the Staring Spotlight and the Stripmap mode, respectively. In Figure 7 the parameter Δ_az represents an offset in azimuth direction with respect to the scenes center coordinate. Analyzing how ambiguities vary from the scene center is essential to ensure good performance throughout the whole image. The AASR performance for Stripmap is smoothly improving for increasing PRFs. However, for Staring Spotlight, there is a dramatic increase in the ambiguity power for low PRFs and especially for targets further away from the scene center.

Figure 7 suggests that the azimuth scene extent of the Staring Spotlight image may be strongly limited by ambiguities. Therefore, the lower bound of the effective PRF has been chosen to be around 2500 Hz to avoid these strong azimuth ambiguities. The upper bound is defined not only by strong RASR in the Stripmap scene but also by satellite limitations. Figure 5 depicts strong RASR for high combined PRFs, but with no indication of a sharp increase with higher PRFs. Therefore, the upper bound of the combined PRF has been chosen to be the maximum PRF of the satellite, which is around 6700 Hz. This results in a usable PRF range for the concurrent mode of $f_\mathrm{PRF} = [5000, ..., 6700]$ Hz or equivalently
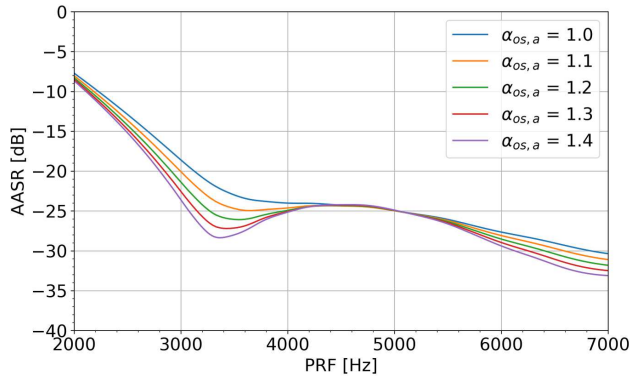
Fig. 8. Simulated AASR for the TerraSAR-X Stripmap mode for different azimuth oversampling factors $\alpha_{\text{os,a}}$. A generalized Hamming window with $\alpha = 0.6$ was used. For the concurrent imaging case, the effective PRF was used.

$$f_{\text{PRF,eff}} = [2500, ..., 3350]\ \text{Hz}.$$

III. COVERAGE ANALYSIS

The timing and ambiguity assessments present several constraints and restrictions intrinsic to the concurrent imaging mode. Consequently, the range of operation in terms of PRF is quite limited. Depending on the target position and the desired scene size, the concurrent acquisition may not even be possible over some locations. This questioning of whether an area can be imaged using the concurrent mode or not, i.e., if a concurrent acquisition on a given target can be performed, motivates a global coverage analysis. This section has the objective to assess the availability of concurrent imaging all over the Earth in a statistical sense.

Before describing the simulations, the term *availability* must be defined. An acquisition is said to be *available* when at least one valid PRF can be found in the PRF table on-board the satellite to perform the concurrent mode. A valid PRF is obtained by respecting all the timing and ambiguity constraints. From a timing point of view, the incidence angle and the PRF together have to be in accordance with the timing diagram. This means that the target echo reception must not interfere with the nadir echo nor with the radar transmission. Besides, due to commanding restrictions, the radar must receive with the same antenna pattern as the previous transmit one at each PRI. In the time domain, this restriction can be translated as having an even number of traveling pulses at the moment of reception of each individual mode. Ambiguities, on the other hand, impose a minimum PRF of 5000 Hz in order to avoid facing strong azimuth ambiguities in the Staring Spotlight acquisition. This minimum PRF value was arbitrarily chosen and can be seen as a lower boundary representing the worst case of the Staring Spotlight azimuth ambiguity.

Among the many possibilities provided by the concurrent imaging technique, one of the most important is the ability to acquire data over two different places at the same time. Once each individual mode uses its own antenna pattern, the targets of each mode can be even hundreds of kilometers apart. This motivates the differentiation between *overlapping concurrent*
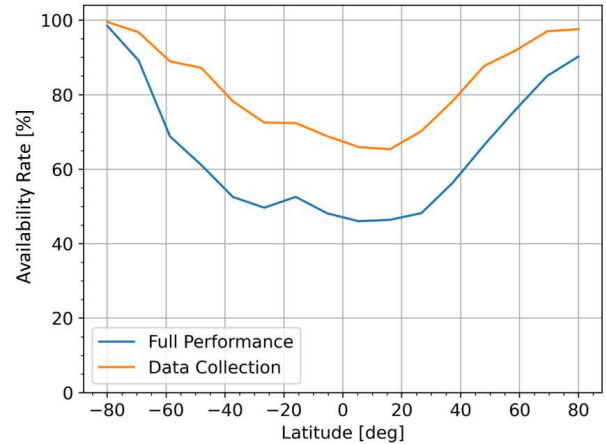

Fig. 9. Availability rate in terms of latitude for the overlapping concurrent mode. The plot represents the probability of a random point at a certain latitude to be accessible for a concurrent acquisition. The blue line represents the full performance incidence angle range, while the orange line represents the data collection range [10].

imaging and *non-overlapping concurrent imaging*. The *overlapping* definition is used when the Staring Spotlight scene is completely within the Stripmap one. The *non-overlapping* definition is used otherwise.

A. Overlapping Concurrent Imaging

Initially, a simulation for the overlapping concurrent mode will be described. This first simulation consists of checking if a random target on Earth can be imaged with a scene size of at least 30 km around the target. In other words, testing if it is possible to perform a concurrent acquisition with a minimum swath width of the Stripmap mode of 30 km being the target in the scene center. The swathes in this simulation are not aligned with the operational TerraSAR-X Stripmap mode swathes but centered around the target of interest. The elevation beam is selected by optimizing the antenna gain over the imaged scene. As the Staring Spotlight has a lower swath width, approximately 5 km, its timing does not need to be checked as its scene is within the Stripmap one. Simulating one hundred thousand random points on Earth's surface and using the TerraSAR-X orbit, the result presented in Figure 9 was obtained. In the plot, 'Full Performance' stands for the simulation in which the incidence angle range of the target is between 20° and 45°, while in 'Data Collection,' this range is extended to 14° and 60°. Those definitions are in line with the basic SAR products' definition of TerraSAR-X [10]. Allowing for a broader range of incidence angles, naturally, the availability increases as there are more acquisition possibilities.

The motivation to plot the availability rate in terms of latitude comes from the geometry of the orbit of the satellite. As a consequence of the polar dusk-dawn orbit, the radar flies over a random point at a high latitude much more frequently than over a point at a lower latitude [27]. The converging orbits towards higher latitudes result in an increased number of acquisition possibilities for high latitudes and a lower
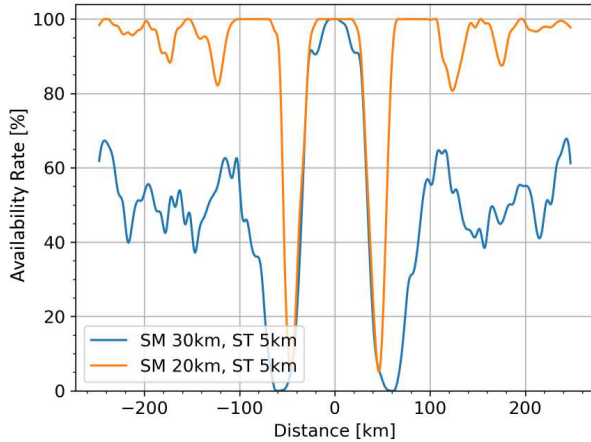
Fig. 10. Availability rate in terms of the distance between the targets for the non-overlapping concurrent imaging mode. The plot represents the probability of random points on the equatorial line to be accessible for different Stripmap scene sizes.

availability rate at the equator. This can be confirmed by the plot presented in Figure 9.

There are two main conclusions from the results obtained. First, the idea that the worst-case scenario of the concurrent imaging mode is approximately at the equator is confirmed. The non-overlapping concurrent mode simulation, therefore, will be run at a latitude of zero degrees. Second, in the full performance range, the worst case of the availability is 45%. The scene size of the non-accessible targets could be reduced to satisfy timing constraints and allow for the acquisition. However, this limitation can also be improved by using certain techniques. For example, by using different PRIs in each mode, as described in Section VI, it would be possible to increase the Stripmap echo window and, consequently, its scene size.

B. Non-Overlapping Concurrent Imaging

The non-overlapping concurrent imaging simulation is related to the non-overlapping availability rate, i.e., when the acquisition is performed over disjunctive scenes. In this case, not only the scene extent of each mode must be defined but also the distance between the targets. Besides, now the targets must only be within the scenes, not necessarily in their centers. From what was learned in the first simulation, now both targets are at the equatorial line, and only the data collection incidence angle range was simulated. This represents the worst case on Earth while using the full capabilities of the satellite. Once again, the simulation tests if the targets are accessible in the non-overlapping way. Using 30 km for the Stripmap scene and 5 km for the Staring Spotlight one, which are nominal values for the satellite, the result shown in Figure 10 by the blue line was obtained. Twenty thousand points were simulated.

The first interesting observation from the image is obtained at distances around zero kilometers, in which the non-overlapping availability rate deteriorates into an overlapping

one. Removing the constraint of the targets being in the scene center, now the availability rate is much higher, at 100%.

The low rate for targets situated between 20 km and 65 km is another interesting point. This effect is mostly caused by the fact that the radar cannot receive while transmitting. In the time domain, this means that the receive echo window is limited by the transmit pulse. Targets that are in this prohibitive distance range mostly represent that one of their echoes is being received while the radar is transmitting.

For even larger distances, the rate goes down to approximately 50%. Once again, these targets can be imaged using the concurrent mode by reducing the Stripmap scene size. For instance, the orange line in Figure 10 represents the same simulation but with the Stripmap swath width reduced to 20 km. The availability rate is considerably improved.

In summary, the Earth coverage analysis described above reveals the good versatility of the concurrent imaging technique. Even though two acquisitions are being performed simultaneously and the timings are quite tight, the mode can still be vastly used around the globe with nominal performance and reasonable coverage. In those extreme cases in which the nominal performance is not possible, the concurrent mode can still be applied simply by slightly reducing the Stripmap scene size. Additional optimization potential is discussed in Section VI.

IV. Experiment Commanding and Processing Approach

For the commanding of a concurrent acquisition, many capabilities offered by the TerraSAR-X instrument have to be used. A concurrent Stripmap/Spotlight acquisition exploits the azimuth antenna steering capabilities employed for the Staring Spotlight mode and the ability for a pulse-to-pulse change of the elevation beam and the used waveform. Due to the large azimuth antenna steering range and the quantization of the antenna steering angles, the Staring Spotlight mode utilizes a substantial part of the instrument's state machine for the azimuth antenna steering [7].

Despite the fact that the TerraSAR-X radar system is designed only for a sequential switching of antenna beams, like for a Spotlight acquisition, it is technically possible to switch to a single dedicated antenna configuration at any time. This capability is semi-operationally used for the so-called aperture-switching acquisitions, providing two phase centers for along-track interferometry applications [28], [29]. However, the aperture-switching mode only toggles between two antenna configurations. The concurrent mode commanding strategy described here is the first time the sequential beam steering of a Spotlight acquisition and the antenna beam toggling of the aperture-switching scheme are combined.

The concurrent imaging technique is not only demanding from an antenna steering point of view but also because the waveforms employed for the Stripmap and the Staring Spotlight mode are tailored for each mode separately and therefore are different. For example, the Staring Spotlight part requires a high range bandwidth of 300 MHz compared to 150 MHz or 100 MHz for the Stripmap acquisition. Additionally, the

chirp slopes are configured in opposite directions for Stripmap and Staring Spotlight within the concurrent acquisition to improve the range ambiguity performance for point targets [21]. The use of different waveforms leads to the necessity of recording two different calibration and replica retrieval sequences, one for each waveform, as shown on the top of Figure 11. The calibration sequence is used for the internal instrument calibration, whereas the replica retrieval sequence provides the matched filter for range focusing [30], [31].

For the processing of the acquired and dumped SAR data on ground, a pre-processing approach is used. As shown in the bottom part of Figure 11, the concurrent imaging SAR raw data is split into two data streams by a pre-processing step, re-arranging the raw data. Those data streams are directed to two standard processors, one configured for Stripmap and the other configured for the Staring Spotlight acquisition. For the experiments shown in Section V, the TAXI processor of the Microwaves and Radar Institute of DLR was used [32]. However, also the operational TerraSAR-X multi-mode SAR processor (TMSP) could be used [33].

For the pre-processing, detailed knowledge of the commanding of the concurrent acquisition is necessary. Although the imaging pulses are simply alternating between the Staring Spotlight and the Stripmap mode data, the auxiliary data is not, as shown in the top row of Figure 11. In the so-called prolog and epilog, sequences of calibration and replica retrieval pulses are contained and have to be directed to the correct data stream for proper processing. The timestamps of the recorded range lines have to be preserved as they contain the information about the orbit position. In addition, for example, the PRF contained in the header of the SAR pulses has to be adapted as only every second pulse of the imaging part is used for each image.

Even though the acquisitions presented here are experiments, the same processing approach could be used for operational implementation. Thereby, the existing processing capabilities, optimized for both modes independently, could be re-used extensively. Only the relatively low complexity pre-processing step described above is necessary.

V. EXPERIMENTAL RESULTS

In order to demonstrate the feasibility and also to highlight the capabilities of the concurrent imaging technique, several experimental acquisitions have been commanded, executed, and evaluated, employing the TerraSAR-X satellite SAR system. Those images can be evaluated for their impulse response function (IRF) characteristics as well as for their ambiguity performance.

A. IRF Analysis

The first experimental acquisition is a TerraSAR-X Staring Spotlight combined with a Stripmap acquisition. In Figure 12 the blue polygon represents the expected coverage of the Stripmap part, whereas the red polygon represents the Staring Spotlight coverage.

The focused images of the experimental acquisition are depicted in Figure 13. The left image is the Stripmap part
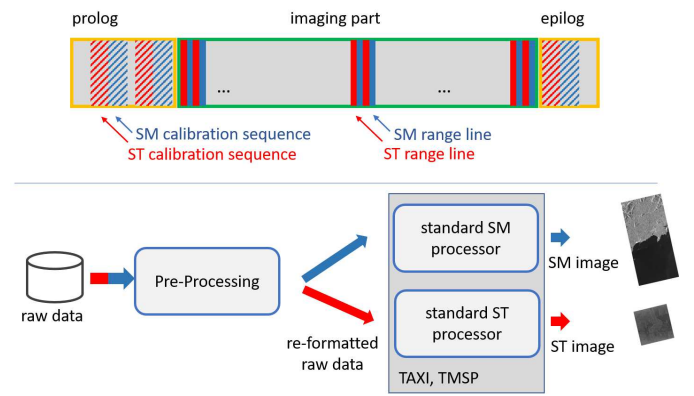

Fig. 11. The upper image shows the structure of the concurrent imaging technique raw data. The actual imaging sequence is shown as green box, containing alternately ST and SM range lines. This imaging sequence is surrounded by a prolog and a epilog, where calibration sequences are contained and the replica for range focusing is acquired. These parts are shown as orange boxes. The lower image shows a block diagram of the concurrent mode processing. The combined raw data is split into two data streams and fed into two processors. One is configured for the Stripmap, the other for the Staring Spotlight part. Finally two images are created.
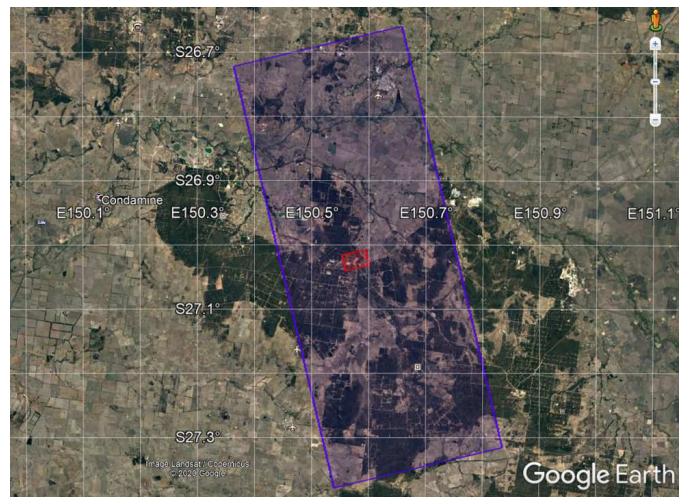

Fig. 12. Polygons of the concurrent acquisition over an area in East Australia, where radar reference targets are deployed (corner reflectors). The blue polygon represents the area which is acquired in Stripmap mode, while the smaller red polygon represents the area imaged in Staring Spotlight mode.

which is characterized by medium resolution but relatively high areal coverage. The upper right image represents the Staring Spotlight part of the acquisition, characterized by high spatial resolution, but reduced areal coverage. The Staring Spotlight area is marked in the Stripmap image by the yellow rectangle in order to highlight the difference in coverage. In order to demonstrate the high resolution capability of the Staring Spotlight part of the acquisition, a corner reflector was imaged. The corner reflector is part of the Australian corner reflector array, located in Surat Basin, Queensland [34], [35]. By evaluating the characteristics of this artificial target, an assessment of the IRF characteristics is possible. A zoom in on the corner reflector in the Staring Spotlight image is also shown. The position of the corner reflector is highlighted by

Fig. 13. The Stripmap part of the experimental acquisition is highlighted with a blue box (left). The yellow rectangle in this image highlights the area, where the Staring Spotlight image is located. The Staring Spotlight part of the experimental acquisition, highlighted by a red box (upper right) offers higher resolution but a smaller scene size (3.5 km × 3.5 km) compared to the Stripmap (22.9 km × 46.5 km). Both images contain a corner reflector, highlighted by the red arrows. The zoomed region of the Staring Spotlight image clearly shows the response of the corner reflector. The Stripmap image is acquired with elevation beam strip_011 and the Staring Spotlight image with elevation beam spot_051 at an incidence angle of about 40°. The acquisition was performed on 2020-07-08.
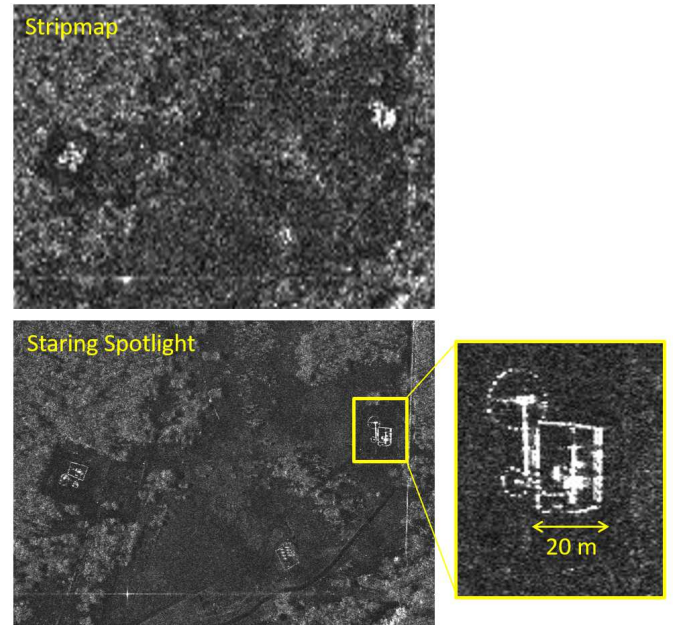

Fig. 14. Zoom in on the area around the corner reflector of the acquisition shown in Figure 13. The corner reflector is visible in the lower left part of the Stripmap (top) and the Staring Spotlight (bottom) scenes. A further zoom in on a man-made structure in the Staring Spotlight scene demonstrates the ability to resolve very detailed structures, e.g., of buildings with this mode.

TABLE I
IMPULSE RESPONSE FUNCTION PARAMETERS EVALUATED FROM THE
CORNER REFLECTOR WITHIN THE IMAGE.

Parameter	conc.-ST	ST	conc.-SM	SM
Res. (az.)	0.229 m	0.219 m	2.767 m	2.982 m
Res. (rg.)	0.573 m	0.595 m	1.785 m	1.767 m
PSLR (az.)	25.7 dB	31.6 dB	28.3 dB	29.3 dB
PSLR (rg.)	24.0 dB	31.3 dB	29.0 dB	30.0 dB
ISLR (az.)	24.7 dB	25.2 dB	20.5 dB	22.4 dB
ISLR (rg.)	21.6 dB	25.4 dB	20.4 dB	22.3 dB

red arrows.

A further zoom in on the area around the corner reflector is shown in Figure 14. Here the high resolution capability of the Staring Spotlight mode as shown on the bottom is clearly visible compared to the Stripmap image on the top. This figure highlights the benefit of acquiring a high-resolution image in parallel to the overview image.

To compare the experimental acquisition with nominal TerraSAR-X image products, two nominal images had been ordered additionally. The experiment was executed on 2020-07-08 and offers a Stripmap and a Staring Spotlight image in one overflight. The Staring Spotlight reference and Stripmap reference images were acquired on 2020-07-19 and 2020-07-30, respectively.

In Table I, the IRF parameters of the concurrent imaging approach and the conventional modes are shown. The resolutions in slant range and azimuth as well as the peak-to-side lobe ratio (PSLR) and integrated side lobe ratio (ISLR) are derived by evaluation of the corner reflector. The resolution of the concurrently acquired images matches very well the number derived for the nominal modes for both the Stripmap and the Staring Spotlight part. The azimuth resolution for the concurrent imaging Stripmap part is slightly better, as a higher processed azimuth bandwidth was applied. Residual differences, both in resolution and side lobe ratios can be attributed to the use of an experimental processing environment for the concurrent imaging acquisition. The processor is tailored for high-precision imaging [36], however the input parameters are partially entered manually. The reference acquisitions have been processed using the operational TerraSAR-X processor.

To demonstrate the capability to image disjunctive areas even with different imaging modes in a single overflight by a single-channel SAR system, a second experiment has been conducted. In Figure 15, the polygons highlighting the coverage of both sub-modes of the experimental acquisition are shown. The red rectangle corresponds to the Staring Spotlight part, whereas the blue polygon is the Stripmap part.

The focused images of the second experimental acquisition are depicted in Figure 16. The left image is the Stripmap part. The upper right image represents the Staring Spotlight scene. The Staring Spotlight image is outside the Stripmap and therefore not highlighted within the Stripmap. The same
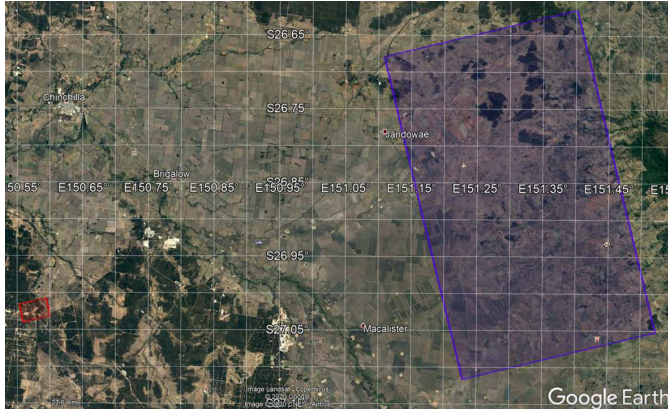
Fig. 15. Polygons of a single-channel concurrent acquisition over an area in East Australia. The blue polygon represents the area which is acquired in Stripmap mode, while the smaller red polygon represents the area imaged in Staring Spotlight mode. For this experiment both parts of the concurrent acquisition are imaging disjunctive areas with different imaging modes.

corner reflector analysis as for the first experiment has been conducted for this experimental acquisition and it supports the observation of comparable resolutions as provided by the reference acquisition.

B. Ambiguity Assessment

To assess the azimuth ambiguity performance and verify the predictions shown in Section II-C, acquisitions over high-contrast scenes have been commanded. A similar analysis as shown in [37] can be carried out to derive the AASR performance. Figure 17 shows a zoom into the Stripmap part of a concurrent acquisition over the municipality of Piúma in the Brazilian state of Espírito Santo. The sea appears dark black and azimuth ambiguities are clearly visible. The arrow highlights a bright area near the coast and its ambiguity in the sea in early azimuth direction. The separation of the actual target and its ambiguity d_{ambi} is about 4 km as expected from

$$d_{\mathrm{ambi}} \approx \frac{f_{\mathrm{PRF}}\lambda R_0 v_{\mathrm{g}}}{2 v_{\mathrm{eff}}^2}, \tag{9}$$

where f_{PRF} is the PRF, v_{g} and v_{eff} are the ground and the effective velocity, respectively. The yellow line indicates where a cut in azimuth direction is used to visualize and analyze the AASR performance. The power of the SAR image along this cut is shown in Figure 18. The power is normalized to the maximum value. The average power of the target area is approximately -1.0 dB, the ambiguity is at -20.0 dB and the sea clutter is at -25.5 dB. By subtracting the sea clutters' power from the value measured at the position of the ambiguity and respecting the target power, an estimate for the AASR of -20.4 dB can be derived. It is important to note that this value is the single sided AASR as the ambiguity power is only coming from the late azimuth direction. For a comparison with the results of Section II-C, 3 dB have to be added, leading to an AASR estimate of -17.4 dB. The value expected from the simulation shown in Section II-C is -19.1 dB for an effective PRF of 3044 Hz.
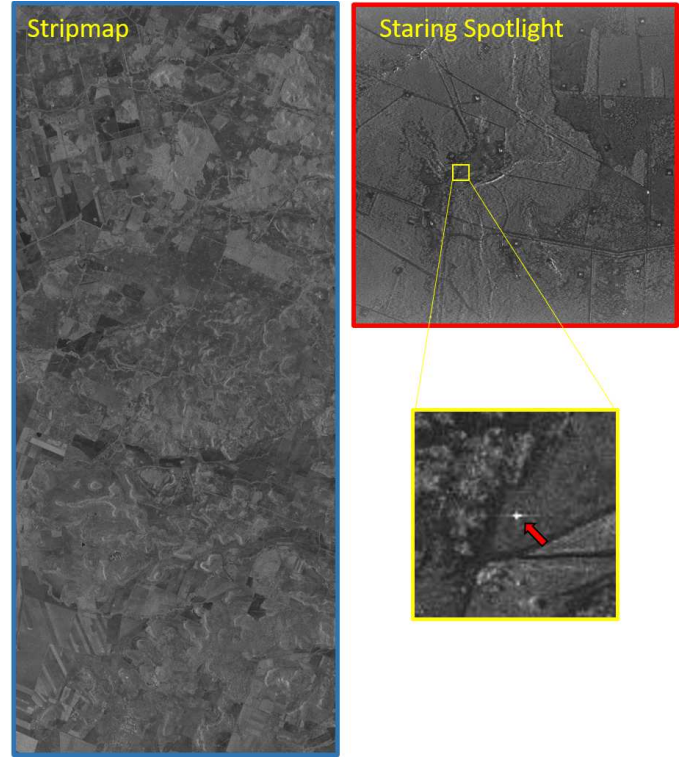

Fig. 16. Stripmap part of the experimental acquisition with a scene size of 20.7 km × 46.5 km (left). The Staring Spotlight part of the experimental acquisition (upper right) is located outside the Stripmap acquisition in this experiment. The scene size is 3.5 km × 3.5 km and the distance between the Stripmap swath and the Staring Spotlight scene is 61 km. The Staring Spotlight is imaging a corner reflector, highlighted by the red rectangle. The zoomed area of the Staring Spotlight image (lower right) clearly shows the response of the corner reflector. The achieved resolution is comparable to the one of the first experiment.

To assess range ambiguities, acquisitions employing the concurrent imaging technique close to the city of Buenos Aires, Argentina have been commanded. In Figure 19 two Stripmap images are shown. The left one is the Stripmap part of a concurrent acquisition performed on 2020-09-24 with elevation antenna beam strip_011. This elevation beam was selected in order to provoke the appearance of range ambiguities in near range, as the antenna gain in near range is degraded compared to a nominal acquisition. The antenna pattern compensation during processing is enhancing the signal energy in the near range area and leads to the dominant appearance of ambiguities. A high ambiguous power especially close to the center in azimuth direction is notable, as highlighted by the yellow box. For comparison the same area was acquired on 2020-10-16 with elevation beam tanDEM_a1_040 as shown on the right of Figure 19. The range ambiguities are very much attenuated compared to the left image. This beam is ideally illuminating the area of interest and would be used for an operational acquisition, e.g., for the bistatic TanDEM-X mission.

In order to analyze the ambiguities recognized in the yellow box of Figure 19 a spectrogram of a single range line is shown in Figure 20. The spectrogram highlights the time-frequency relations of the analyzed signal. In the lower part, a linear
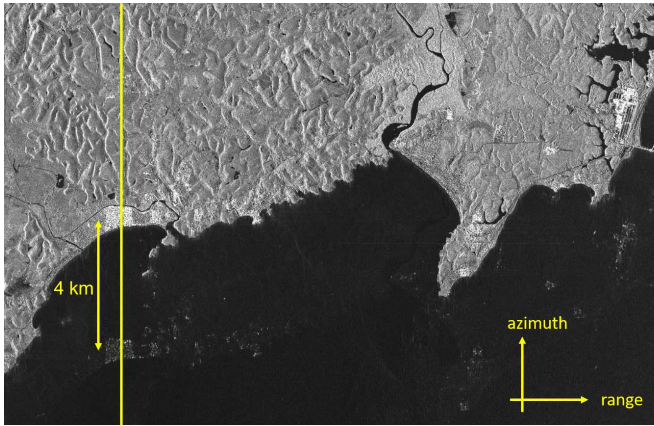
Fig. 17.   Zoom into the Stripmap part of a concurrent acquisition acquired over the municipality of Piúma in the Brazilian state of Espírito Santo. The sea during the acquisition was very calm. Therefore, it appears dark black. At the coast, a bright area is visible. Its first ambiguity repeats in the sea at a distance of about 4 km, according to the PRF. A cut in the azimuth direction, indicated by the yellow line, is used to assess the AASR performance, as shown in Figure 18.
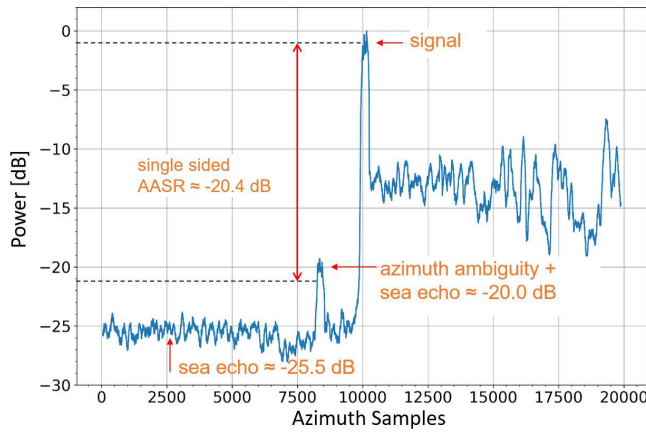

Fig. 18.   Azimuth profile along the sea-land transition (yellow line in Figure 17) for the Stripmap part of the concurrent acquisition used to evaluate the azimuth ambiguity performance.
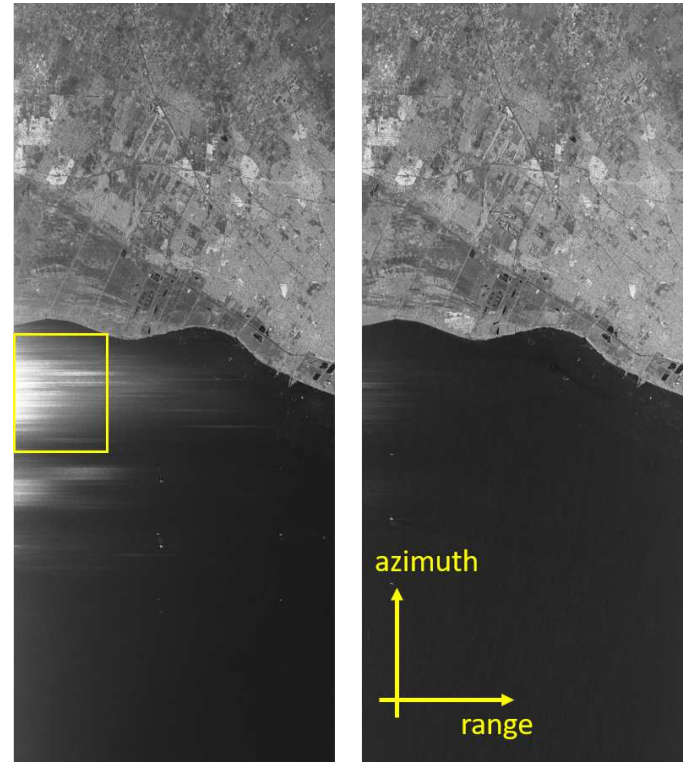

Fig. 19.   Stripmap images of two concurrent acquisitions close to the city of Buenos Aires, Argentina. The left image was acquired on 2020-09-24 using elevation beam strip_011. This beam results in reduced antenna gain in near range, leading to the exaggeration of ambiguous signals here. The right image was acquired on 2020-10-16, using elevation beam tanDEM_a1_040. This beam is ideally illuminating the scene and provides an almost ambiguity-free image. This beam would be the choice for an operational acquisition.
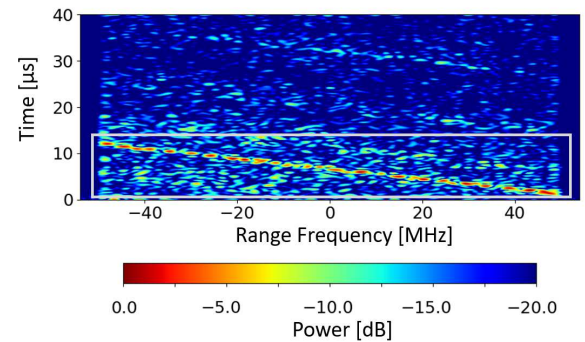

Fig. 20.   Spectrogram of a single range line of the raw data in the area highlighted by the yellow box in Figure 19. The white box highlights the response of a dominant target in the ambiguous range with a clear down chirp characteristic. A chirp rate analysis reveals, that the ambiguous signal in the Stripmap image originates from a Staring Spotlight pulse.

frequency slope is clearly visible as highlighted by the white box. The clear visibility of a line is an indicator for a dominant target within the ambiguous range. The chirp rate of the down chirp can be estimated from the bandwidth of 100 MHz and the duration of approximately 11 µs as 9.1 MHz/µs. This estimate corresponds very well to the chirp rate of the Staring Spotlight part of the concurrent acquisition which employs a down chirp waveform with 9.28 MHz/µs. This confirms that the ambiguity within the Stripmap image is caused by a Staring Spotlight pulse. The power of the ambiguity is already reduced by a factor of three compared to the actual power of the Staring Spotlight pulses' echo. This is because the Stripmap receive signal is filtered to 100 MHz and the actual interfering signal is transmitted with 300 MHz bandwidth. Additionally, the ambiguity is not focusing in range, as the chirp slopes of the Stripmap and the Staring Spotlight part were chosen opposite to smear the response of ambiguities. Nevertheless,

ambiguity is a dominant disturbance in the image. This provoked ambiguity can be used for further investigations of ambiguity mitigation techniques as described in Section VI.

VI. FURTHER OPTIMIZATION

The results shown in the previous sections are already very promising. Nevertheless, there are opportunities for further improvements, e.g., with respect to ambiguity performance,

swath coverage, and global availability of a potential operational concurrent mode for the TerraSAR-X mission.

Due to the necessity of high PRFs, the concurrent imaging technique is demanding from an ambiguity point of view. However, there are promising techniques to reduce ambiguities. One is the use of waveform encoding and dual-focus processing to reduce range ambiguities [38], [39]. The other is to employ multiple channels in azimuth, probably even in a bi- or multistatic configuration, in order to allow for an azimuth ambiguity suppression [40]–[42]. At the current time, the TerraSAR-X and TanDEM-X satellites are still in close orbit formation. After completing the global digital elevation model (DEM) mission [43]–[45], they are serving a multitude of scientific purposes. This close-formation could serve as an excellent testbed for bistatic concurrent imaging.

Another aspect with optimization potential is the timing. The experiments presented in this paper and the mode described in [18] halved the nominal PRI or doubled the PRF, respectively. However, as shown in the upper row of Figure 21, the Staring Spotlight part of the concurrent acquisition is not as demanding as the Stripmap one concerning the timing. The Stripmap scene is much larger and therefore demands a longer echo window. The Stripmap PRI is completely utilized. The gray bars in the Staring Spotlight PRI highlight spare times. By keeping the effective PRI constant (cf. Equation 2) and decreasing the Staring Spotlight PRI, a longer echo window for the Stripmap part can be achieved, as shown in the lower part of Figure 21. In this example, an improvement of 17.7% of the Stripmap swath width can be achieved. The unused times during the Staring Spotlight PRI are significantly reduced. It is not completely vanishing, as the PRI could not be reduced further because the maximum available PRF of TerraSAR-X is around 6700 Hz, leading to a minimum PRI of about 149 μs. For improving the Stripmap echo window length, only the spare time after the echo window extension of the Staring Spotlight can be used. The spare time before is dictated by the effective PRF and the position of the Staring Spotlight scene. Also, an increase of the Staring Spotlight echo window to acquire a larger scene is not possible, as the constraining factor here is the produced amount of data and the data rate. Staring Spotlight is using 300 MHz range bandwidth, requiring a high sampling frequency which in turn produces a large data rate for the solid state mass memory and its interface [7].

In Section II, a concurrent Stripmap/Spotlight mode using the TerraSAR-X Staring Spotlight mode and a two-beam Stripmap were discussed. However, also a concurrent Stripmap/Spotlight using the TerraSAR-X High-Resolution Spotlight mode can be investigated in more detail in the future. It can further enlarge the trade space of resolution against ambiguity performance. The High-Resolution Spotlight mode is a Sliding Spotlight variant and offers decreased azimuth resolution compared to Staring Spotlight, but with improved azimuth ambiguity performance and azimuth scene size.

VII. CONCLUSION

In this paper, we describe a concurrent imaging technique that can acquire two SAR images simultaneously by a pulse-to-pulse interleaving of both imaging modes. The mode is able
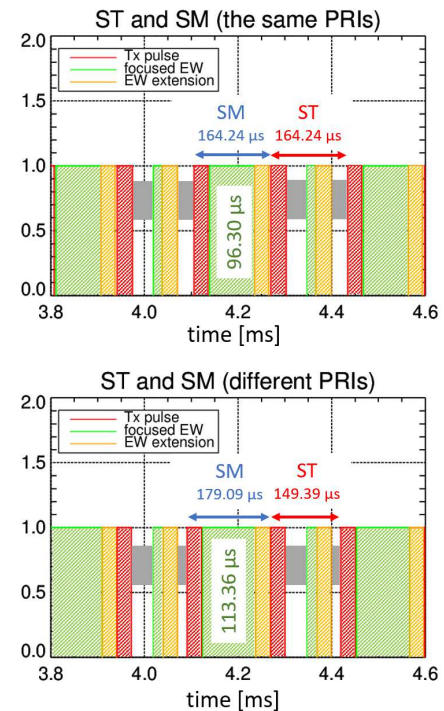

Fig. 21. Sequence of alternating Stripmap and Staring Spotlight pulses of the concurrent acquisition shown in Figure 13 (top). Transmitted pulses are shown in red. The focused echo window length is shown in green, whereas the echo window extension, necessary for matched filtering in range, is shown in orange color. For the used PRF of 6088.55 Hz a PRI of 164.24 μs enables a focused echo window length of 90.30 μs for the Stripmap. The gray bars highlight unused times during the Staring Spotlight PRI. Using different PRIs for the Stripmap and the Staring Spotlight part, while keeping the same effective PRF, enables a longer echo window for the Stripmap, while leaving the Staring Spotlight scene unchanged (bottom). An improvement of 17.7 % in the Stripmap scene size is achieved by reducing the unused times during the Staring Spotlight PRI (gray bars).

to acquire an overview image in Stripmap mode and, at the same time, provides a zoom on a target of high interest, e.g., an airfield, power plant, or other critical infrastructure. Because of the pulse-to-pulse interleaving, the mode is complex in terms of timing and ambiguity performance. We provide a thorough analysis of these aspects for the TerraSAR-X case. Additionally, an analysis of the global availability of concurrent acquisitions demonstrates the potential of this mode even on a global scale. For high and medium latitudes an availability of concurrent mode data of more than 70% can be achieved. Commanding and processing aspects are discussed and the approach of using a pre-processing step together with the already established TerraSAR-X processor environments is shown. The experimental acquisitions and the analysis w.r.t. impulse response function and ambiguity characteristics highlight that the expected performance could be achieved. The results demonstrate the potential of this mode. By compromising scene size and ambiguity performance in a very controlled way, two SAR products can be acquired at the same time, either on the same, or over disjunctive areas, as desired by the customer. Besides the already achieved promising results, there are ideas for further improvements

that will be investigated in the near future.

REFERENCES

[1] I. Cumming and F. Wong, *Digital Signal Processing of Synthetic Aperture Radar Data: Algorithms and Implementation*, ser. Artech House signal processing library. Artech House, Incorporated, 2005.

[2] J. Curlander and R. McDonough, *Synthetic Aperture Radar: Systems and Signal Processing*, ser. Wiley Series in Remote Sensing and Image Processing. Wiley, 1991.

[3] W. G. Carrara, R. S. Goodman, and R. M. Majewski, *Spotlight Synthetic Aperture Radar*. Norwood, MA: Artech House, 1995.

[4] F. De Zan and A. M. Guarnieri, "TOPSAR: Terrain observation by progressive scans," *IEEE Trans. Geosci. Remote Sens.*, vol. 44, no. 9, pp. 2352–2360, 2006.

[5] A. Meta, J. Mittermayer, P. Prats, R. Scheiber, and U. Steinbrecher, "TOPS imaging with TerraSAR-X: Mode design and performance analysis," *IEEE Trans. Geosci. Remote Sens.*, vol. 48, no. 2, pp. 759–769, 2009.

[6] J. Mittermayer, S. Wollstadt, P. Prats, and R. Scheiber, "The TerraSAR-X staring spotlight mode concept," *IEEE Trans. Geosci. Remote Sens.*, vol. 52, no. 6, pp. 3695–3706, 2014.

[7] T. Kraus, B. Bräutigam, J. Mittermayer, S. Wollstadt, and C. Grigorov, "TerraSAR-X staring spotlight mode optimization and global performance predictions," *IEEE J. Sel. Topics Appl. Earth Observations Remote Sens.*, vol. 9, no. 3, pp. 1015–1027, 2015.

[8] D. Belcher and C. Baker, "High resolution processing of hybrid stripmap/spotlight mode SAR," *Proc. Inst. Electr. Eng.–Radar, Sonar Navig.*, vol. 143, no. 6, pp. 366–374, 1996.

[9] G. Franceschetti, R. Guida, A. Iodice, D. Riccio, and G. Ruello, "Efficient simulation of hybrid stripmap/spotlight SAR raw signals from extended scenes," *IEEE Trans. Geosci. Remote Sens.*, vol. 42, no. 11, pp. 2385–2396, 2004.

[10] T. Fritz and M. Eineder, "TerraSAR-X basic product specification document," *DLR Public Document TD-GS-PS-3302*, no. 1.9, 2013.

[11] G. Krieger, N. Gebert, and A. Moreira, "Multidimensional waveform encoding: A new digital beamforming technique for synthetic aperture radar remote sensing," *IEEE Trans. Geosci. Remote Sens.*, vol. 46, no. 1, pp. 31–46, 2008.

[12] ——, "Hochauflösendes Synthetik-Apertur-Seitensicht-Radarsystem mittels Digital Beamforming," *German Patent Application DE*, vol. 10, p. 022, 2006.

[13] G. Krieger, "MIMO-SAR: Opportunities and pitfalls," *IEEE Trans. Geosci. Remote Sens.*, vol. 52, pp. 2628–2645, 2014.

[14] S. Bertl, P. Lopez-Dekker, S. Wollstadt, and G. Krieger, "Demonstration of digital beamforming in elevation for spaceborne synthetic aperture radar," in *Proc. EUSAR*, Berlin, Germany, 2014, pp. 205–208.

[15] T. Fritz and M. Eineder, "TerraSAR-X basic product specification document," German Aerospace Center (DLR), Tech. Rep. 1.9, 2013. [Online]. Available: http://terrasar-x.dlr.de/pdfs/TX-GS-DD-3302_1.9.pdf

[16] M. Adolph, U. Hackenberg, R. Reber, R. Rieger, B. Schweizer, B. Adelseck, H. Brugger, and M. Lorcher, "High-precision temperature drift compensated t/r-module for satellite based sar applications," vol. 2. Paris, France: IEEE, 2005, pp. 4 pp.–816.

[17] M. Porfilio, S. Serva, C. A. M. Fiorentino, and D. Calabrese, "The acquisition modes of COSMO-SkyMed di Seconda Generazione: A new combined approach based on SAR and platform agility," in *Proc. IEEE Geosci. Remote Sens. Symp. (IGARSS)*, 2016, pp. 2082–2085.

[18] D. Calabrese, V. Mastroddi, S. Federici, and S. Serva, "Discrete stepped strip (DI2S) for multi-swath acquisitions," in *Proc. APSAR*, 2015, pp. 191–195.

[19] D. Calabrese, V. Mastroddi, and S. Federici, "DI2S multiswath innovative technique for SAR acquisitions optimization," *IEEE Geosci. Remote Sens. Lett.*, vol. 14, no. 10, pp. 1820–1824, 2017.

[20] D. Calabrese, "Multiple-swath stripmap SAR imaging," Jan. 16 2018, US Patent 9,869,764.

[21] J. Mittermayer and J. M. Martínez, "Analysis of range ambiguity suppression in SAR by up and down chirp modulation for point and distributed targets," in *Proc. IEEE Geosci. Remote Sens. Symp. (IGARSS)*, vol. 6, 2003, pp. 4077–4079.

[22] S. Wollstadt and J. Mittermayer, "Nadir margins in TerraSAR-X timing commanding," *Proceedings of the Committee on Earth Observation Satellites (CEOS)*, p. 4, 2008.

[23] J. Balkoski and F. Bordoni, "Nadir echo properties, a study based on TerraSAR-X data," in *Proc. 20th Telecommunications Forum (TELFOR)*, 2012, pp. 420–423.

[24] D. Massonnet and J.-C. Souyris, *Imaging with Synthetic Aperture Radar*. CRC Press, 2008.

[25] S. Brusch, S. Lehner, T. Fritz, M. Soccorsi, A. Soloviev, and B. van Schie, "Ship surveillance with TerraSAR-X," *IEEE Trans. Geosci. Remote Sens.*, vol. 49, pp. 1092–1103, 2011.

[26] M. Bachmann, M. Schwerdt, and B. Bräutigam, "Accurate antenna pattern modeling for phased array antennas in SAR applications - demonstration on TerraSAR-X," *International Journal of Antennas and Propagation*, vol. 2009, pp. 1–9, 2009.

[27] S. D'Amico, C. Arbinger, M. Kirschner, and S. Campagnola, "Generation of an optimum target trajectory for the TerraSAR-X repeat observation satellite," in *Proc. 18th International Symposium on Space Flight Dynamics*, Munich, Germany, 2004.

[28] H. Runge, C. Laux, M. Gabele, R. Metzig, U. Steinbrecher, R. Romeiser, and M. Gottwald, "Performance analysis of virtual multi-channel modes for TerraSAR-X," in *Proc. EUSAR*, vol. 6, 2006.

[29] S. Suchandt, H. Runge, H. Breit, U. Steinbrecher, A. Kotenkov, and U. Balss, "Automatic extraction of traffic flows using TerraSAR-X along-track interferometry," *IEEE Trans. Geosci. Remote Sens.*, vol. 48, no. 2, pp. 807–819, 2010.

[30] M. Schwerdt, B. Bräutigam, M. Bachmann, B. Döring, D. Schrank, and J. H. Gonzalez, "Final TerraSAR-X calibration results based on novel efficient methods," *IEEE Trans. Geosci. Remote Sens.*, vol. 48, no. 2, pp. 677–689, 2009.

[31] B. Bräutigam, J. H. Gonzalez, M. Schwerdt, and M. Bachmann, "TerraSAR-X instrument calibration results and extension for TanDEM-X," *IEEE Trans. Geosci. Remote Sens.*, vol. 48, no. 2, pp. 702–715, 2009.

[32] P. Prats, M. Rodriguez-Cassola, L. Marotti, M. Naninni, S. Wollstadt, D. Schulze, N. Tous-Ramon, M. Younis, G. Krieger, and A. Reigber, "TAXI: A versatile processing chain for experimental TanDEM-X product evaluation," in *Proc. IEEE Geosci. Remote Sens. Symp. (IGARSS)*, 2010, pp. 4059–4062.

[33] H. Breit, T. Fritz, U. Balss, M. Lachaise, A. Niedermeier, and M. Vonavka, "TerraSAR-X SAR processing and products," *IEEE Trans. Geosci. Remote Sens.*, vol. 48, no. 2, pp. 727–740, 2010.

[34] M. Garthwaite, S. Nancarrow, A. Hislop, M. Thankappan, J. Dawson, and S. Lawrie, "The design of radar corner reflectors for the Australian geophysical observing system: a single design suitable for InSAR deformation monitoring and SAR calibration at multiple microwave frequency bands," *Geoscience Australia, Canberra*, no. Record 2015/03, 2015.

[35] M. Garthwaite, M. Hazelwood, S. Nancarrow, A. Hislop, and J. Dawson, "A regional geodetic network to monitor ground surface response to resource extraction in the northern Surat Basin, Queensland," *Australian Journal of Earth Sciences*, vol. 62, no. 4, pp. 469–477, 2015.

[36] P. Prats, R. Scheiber, M. Rodríguez-Cassolà, S. Wollstadt, J. Mittermayer, B. Bräutigam, M. Schwerdt, A. Reigber, and A. Moreira, "High precision SAR focusing of TerraSAR-X experimental staring spotlight data," in *Proc. IEEE Geosci. Remote Sens. Symp. (IGARSS)*, Munich, Germany, 2012, pp. 3576–3579.

[37] T. Kraus, G. Krieger, M. Bachmann, and A. Moreira, "Spaceborne demonstration of distributed SAR imaging with TerraSAR-X and TanDEM-X," *IEEE Geosci. Remote Sens. Lett.*, vol. 16, no. 11, pp. 1731–1735, 2019.

[38] M. Villano, G. Krieger, and A. Moreira, "Nadir echo removal in synthetic aperture radar via waveform diversity and dual-focus postprocessing," *IEEE Geosci. Remote Sens. Lett.*, vol. 15, no. 5, pp. 719–723, 2018.

[39] ——, "Waveform-encoded SAR: A novel concept for nadir echo and range ambiguity suppression," in *Proc. EUSAR*, 2018, pp. 1–6.

[40] G. Krieger, N. Gebert, and A. Moreira, "Unambiguous SAR signal reconstruction from nonuniform displaced phase center sampling," *IEEE Geosci. Remote Sens. Lett.*, vol. 1, no. 4, pp. 260–264, 2004.

[41] N. Gebert, G. Krieger, and A. Moreira, "Digital beamforming on receive: Techniques and optimization strategies for high-resolution wide-swath

SAR imaging," *IEEE Trans. Aerosp. Electron. Syst.*, vol. 45, no. 2, pp. 564–592, 2009.

[42] T. Kraus, G. Krieger, M. Bachmann, and A. Moreira, "Spaceborne demonstration of distributed SAR imaging with TerraSAR-X and TanDEM-X," *IEEE Geosci. Remote Sens. Lett.*, vol. 16, no. 11, pp. 1731–1735, 2019.

[43] G. Krieger, A. Moreira, H. Fiedler, I. Hajnsek, M. Werner, M. Younis, and M. Zink, "TanDEM-X: A satellite formation for high-resolution SAR interferometry," *IEEE Trans. Geosci. Remote Sens.*, vol. 45, no. 11, pp. 3317–3341, 2007.

[44] M. Zink, M. Bachmann, B. Bräutigam, T. Fritz, I. Hajnsek, A. Moreira, B. Wessel, and G. Krieger, "TanDEM-X: The new global DEM takes shape," *IEEE Geosci. Remote Sens. Mag.*, vol. 2, no. 2, pp. 8–23, 2014.

[45] P. Rizzoli, M. Martone, C. Gonzalez, C. Wecklich, D. B. Tridon, B. Bräutigam, M. Bachmann, D. Schulze, T. Fritz, M. Huber *et al.*, "Generation and performance assessment of the global TanDEM-X digital elevation model," *ISPRS J. Photogramm. Remote Sens.*, vol. 132, pp. 119–139, 2017.

Markus Bachmann received the Dipl.-Ing. degree and his PhD degree in electrical engineering from the Technical University of Karlsruhe, Germany, in 2005 and 2015 respectively.

In 2005 he joined the Microwaves and Radar Institute at the German Aerospace Center. From 2005 to 2011 he was in charge of the implementation and calibration of the TerraSAR-X/TanDEM-X antenna model. From 2006 to 2010 he assessed the potentials and methods of the DEM calibration for TanDEM-X. From 2008 to 2010 he was responsible for the planning and execution of the TanDEM-X commissioning phase. Between 2011 and 2014 he performed the interferometric and radargrametric calibration of the TanDEM-X system and established the monitoring of the global coverage for the TanDEM-X mission. He is ground segment project manager of the Tandem-L/Rose-L-Tandem project since 2016. Since 2012, he is head of the Mission Engineering group, which is in charge of the operational planning of the bistatic acquisitions for TanDEM-X and for future missions like Tandem-L, Rose-L Tandem or HRWS as well as for the analysis of mission relevant aspects in the frame of various SAR missions.

Thomas Kraus received the M.Sc. degree in electrical engineering from the University of Ulm, Ulm, Germany, in 2009.

In 2010, he joined the Microwaves and Radar Institute, German Aerospace Center, Oberpfaffenhofen, Germany, where he is currently working in the field of spaceborne SAR. He is involved in the instrument commanding, the processing, and the analysis of scientific and experimental acquisitions in the framework of the projects TerraSAR-X and TanDEM-X. He was responsible for the performance analysis during the operational implementation of the Staring Spotlight and the wide ScanSAR modes of TerraSAR-X as well as the dual receive antenna mode in the bistatic science phase of TanDEM-X. For the geostationary mission proposal Hydroterra he also contributed the SAR performance analysis. His research interests include radar system performance, the development of innovative SAR modes, and the analysis of distributed satellite SAR systems.

Ulrich Steinbrecher received theDipl.-Ing. degree in electrical engineering/communication from the University of Siegen, Siegen, Germany, in 1990.

In 1990, he started his career with the German Aerospace Center, Wessling, Germany, with the development of a SAR raw data simulator. Then, he was in software development with the X-SAR Processor and with the joint U.S.–Italian–German SIRC/XSAR Missions in 1994. When the data were inhouse, he concentrated on aspects of the operational SAR processing of high data volumes. In 1995, he pioneered a completely automatic SAR processing system based on a robotmaintained mass memory archive. Before he became responsible for the development of the raw data analysis and screening system for the shuttle radar topography mission, he developed the software for a phase-preserving ScanSAR processor for Radarsat-1. In the time between the SRTM mission and the start of the TerraSAR-X project, he left the SAR domain for two years and contributed to the SCIAMACHY LIMB processing system. Since 2002, he has been concerned with the TerraSAR-X radar system, and since the launch of the satellite, in 2007, he was responsible for TerraSAR-X instrument operations.

João Pedro Turchetti Ribeiro received the B.S.E.E. degree from the Aeronautics Institute of Technology (ITA), São José dos Campos, Brazil, in 2021. His bachelor thesis focused on a novel concurrent imaging mode capable of performing two acquisitions simultaneously using the satellite TerraSAR-X. The thesis was conducted in partnership with the German Aerospace Center (DLR).

He is currently developing his master thesis at ITA in cooperation with DLR, expecting to conclude the master's degree in 2022. The topic of research is the improvement of the proposed concurrent imaging mode. His research interests include signal processing techniques such as OFDM, space-time coding, and pre-equalization.

Christo Grigorov received the M.Sc. degree in computer science from the Technical University Sofia, Sofia, Bulgaria, in 2005, and the double M.Sc. degree in space science and technology from the Julius-Maximilians University of Wuerzburg, Wuerzburg, Germany and from the Lulea University of Technology, Lulea, Sweden, in 2007.

In 2008, he was with the Microwaves and Radar Institute (HR), German Aerospace Center (DLR), Germany. He has been working as Systems Engineer and Software Engineer for ground segments of radar satellite missions such as TerraSAR-X and TanDEM-X with focus on system design, integration, and implementation of new features. He leads the Systems Engineering team with HR, DLR.

Mr. Grigorov has been a member of the International Council on Systems Engineering since 2009 and a holder of the INCOSE Associate Systems Engineering Professional Certificate.